

氧化鋅奈米結構製作及特性分析之探討

學生：李思毅

指導教授：曾俊元 教授

林 鵬 教授

國立交通大學

工程學院

材料科學暨工程研究所



摘要

本研究以寬能帶的二六族半導體材料中的氧化鋅(ZnO)為主要的研究與探討的目標；在奈米結構的定義上，本研究採用維度限制的觀念，亦即在三個方向(x, y, z 三軸)受到奈米尺度限制(長度在 100 奈米以下)時稱為三維奈米結構(3D-nanostructure)，兩個方向受到限制則稱之為二維奈米結構，如本研究所著重的氧化鋅奈米線，若只有一個維度受到奈米尺度的限制，則為一維奈米結構如現今許多研究中所提到的奈米薄膜；本研究針對氧化鋅奈米線的製作方式，物理性質，化學性質，光學特性及電學特性等作一個全面性的研究與探討，試圖提出幾個氧化鋅奈米線的成長模型與其光學與電學特性的相互影響關係，並且研究其作為場發射平面顯示元件時所須要具備的電學特性指標，同時提出解決的方式與未來研究可進行的方向與內容。

文中採用兩階段氣液固法(2 step Vapor-Liquid-Solid process)來成長氧化鋅奈米線，相較於一般傳統的氣液固法而言，這個改進式的成長方式利用兩階段的升溫方式可以有效的將在基板表面的觸媒金屬薄層形成一些有規則或是尺寸相對較小的奈米金屬觸媒點，接著其後的快速升溫過程可以將溫度迅速的提升到鋅蒸氣產生的溫度範圍，以一個穩定的溫度環境進行飽和析出的氧化鋅奈米線成長過

程，如此可以將其成長出來的氧化鋅奈米線幾何尺寸維持在 80 nm 的直徑與約 5 μm 長度的大小。

在金屬觸媒的使用上，也有很多不同的選擇，傳統的金觸媒較不易成長具有一定有序的氧化鋅奈米線，這是因為金觸媒在與矽基板之共晶溫度時，極易形成不規則的奈米級顆粒，為一個多晶的結構體，造成在氣液固法成長時氧化鋅過飽和析出時的不規則性，以致形成較為雜亂分佈的氧化鋅奈米線。而實驗中所選擇的銅奈米顆粒觸媒點則可以在其與矽基板的共晶溫度形成非常規則的觸媒點，有助於氧化鋅奈米線的有序成長。

在載氣氣氛的選擇上，使用高純度的氰氣作為成長上的氣流控制，不同的氣流流速將會影響到氧化鋅奈米線成長過程中的鋅蒸氣含量多寡與成長，速率較快的流速對於成長出線徑較小的奈米線較有幫助，同時長度上也增長許多，其幾何關係比可以到達的程度，相對於流速較低的環境所成長出的奈米線，其缺陷也因為快速成長而變得較多，在選用高純度氮氣氣氛後，更可以發現因為氮氣本身的黏滯係數較小，進一步加速了氧化鋅奈米線的成長速率，也提高了幾何比，對於光學與電性特性都有一定程度上的增強作用。

肇因於尋求更好的光學激發與電性特性，也有鑑於成長方向雜亂的原因可能為基板與氧化鋅之間的晶格不匹配所致，因此藉著超薄氧化鋅緩衝層的引入，先在矽基板上成長一單晶優選方向(002)的超薄氧化鋅氧化層，接著再依循先前的氣液固方式成長氧化鋅奈米線，發現藉由氧化鋅緩衝層的幫助可以有效的解決晶格不匹配所導致的方向不均與缺陷機制，使氧化鋅奈米線可以垂直的成長於基板之上，不再受到基板方向與晶格的限制，如此可以元件化的氧化鋅奈米線製作成為可能，更可以有效的整合至現今的半導體製程內。

以上的各式不同製程的氧化鋅奈米線其光學激發特性研究方面，藉由光致發光的頻譜配合材料分析工具可以知道當激發光為 325 nm 時其在 380 至 400 nm 的範圍內會有一極為顯著的紫外光激發峰，此峰值的位置反映了氧化鋅奈米線中的結晶情形與雜質分佈，同時也與結晶的缺陷有相當程度的關係，其他的特徵峰值則說明了氧缺陷或是氧空缺以及鋅原子的移動情況。

在場發射特性的探討中，針對不同成長條件下的氧化鋅奈米線測量其場發射特性，可以發現具有垂直方向成長的奈米線其激發電場(trun-on electric field)約為 0.83 V/ μm ，是一項很優異的成果，歸因於相當均一的奈米線成長型態與幾何大小且是完美的單晶晶體，才可以得到如此低的激發電場值，此一數值的有效降低頗具實用價值，意即可以運用較低的電壓來使場發射平面顯示器達到場發射激發的效果，不但可以節省電能更可以提升產品的使用壽命與兼顧環保的需求。藉由分析 Fowler-Nordheim 圖所計算出的場發射增強因子(field emission enhancement factor, β)可以達到 7,180，此以數值與其他場發射奈米線如奈米碳管($\beta \sim 1,100$)比較也已較高，同時也已經達到實用化的範疇。

為了進一步增強氧化鋅奈米線的場發射特性與應用，吾人設法利用摻雜的方式降低氧化鋅本身的阻抗，經實驗證明加入微量的錫(Tin, Sn)有助於降低氧化鋅

奈米線的有效阻抗，此一摻雜證明確實可以降低奈米線的內部阻抗(由未摻雜的 $85.43\text{ k}\Omega$ 降至 $8.53\text{ k}\Omega$)，另一方面由於低熔點金屬錫的加入也間接的降低了氣液固法在成長氧化鋅奈米線時的溫度(由原先的 900 度降至 805 度)，其在場發射特性的表現上，經由摻雜的結果也將原先的機發電場由 $0.83\text{ V}/\mu\text{m}$ 大幅降低至 $0.07\text{ V}/\mu\text{m}$ 附近，藉著良好的低阻抗高方向性成長的錫摻雜氧化鋅奈米線的製作也將場發射幾何增強因子增加到 6.67×10^5 左右，是一個很好的結果。

此外，利用元件製作的技術，吾人成功的製作出一具備有閘極控制的氧化鋅奈米現場發射元件，利用不同的閘極電壓，可以有效的控制氧化鋅奈米線的場發射行為，在量測的數據顯示最佳的控制操作電壓約為 35 伏特，同時最佳的電壓與電流比(Transconductance, g_m)位於 $3.88 \times 10^{-4}\text{ S}$ ，這樣的特性將可以初步的證明氧化鋅奈米線其在接受控制之後可以具備較佳的場發射特性與極為穩定的場發射電流密度，對於未來的場發射顯示元件而言相當的具有實用性的潛力。

經過觸媒金屬選擇，載氣氣氛控制，光學激發特性分析以及場發射性質的研究，可以對現階段的氧化鋅二維奈米結構的成長機制與結晶過程給予一個較為明確的探討，同時也針對未來的場發射平面顯示元件的基礎性研究提供了清楚的模型，證明場發射元件材料可以朝著寬能代半導體材料的領域發展，運用其寬能帶的優良激發特性與奈米結構微型化的相輔相成而早日達到實際應用的領域。



The Synthesis and Characteristics of ZnO Nano Structure

Student: Seu Yi Li

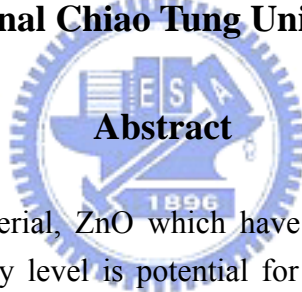
Advisor: Professor Tseung Yuen Tseng

Professor Pang Lin

Materials Science and Engineering Department

Institute of Engineering

National Chiao Tung University



The wide band gap material, ZnO which have 3.37 eV energy band gap and about 60 meV excitation energy level is potential for nano laser application and flat display applications in the future. This research is focus on the 2-D nanostructure which means the x and y axis was limit by the nano size (<100 nm). The characteristics of the ZnO nanowires are paying attention in growth mechanism, optical emission, and electric properties. Furthermore, the field emission devices are also been focus on the low turn-on electric field and more stability current density.

Here we report for the first time the ZnO-nanowire-growth on p-type Si (100) substrates using a VLS process catalyzed by copper instead of gold. This is a new method for preparing ZnO NWs through a rapid and cost effective thermal process. The two-step VLS growth method, used in this study reduced the liquid metal size and content efficiently to promote the growth of ZnO NWs. Furthermore, in this process we introduce the thermal annealing steps to make ZnO NWs approach vertically on the Si substrate.

Among various preparation methods, the metal catalytic VLS growth process provides a cheap and speedy route for large-area deposition of nanowires. The physical structures of the nanowires are affected strongly by the fabricating parameters such as starting materials, temperature, time and atmosphere. However,

the effect of atmosphere on the structure and property of ZnO nanowires was scarcely studied. In the present study, we grow ZnO nanowires on Si (100) p-type substrate by using Cu catalyzed VLS with Ar and N₂ carrying gases. The effects of atmosphere on the morphology, structure and optical property of those nanowires were studied.

The nanowire growth process was controlled by surface morphology and orientation of the epitaxial ZnO buffer layer, which was deposited by radio-frequency (rf) sputtering. The copper catalyzed the vapor-liquid-solid growth of ZnO nanowires with diameter of ~ 30 nm and length of ~ 5.0 μm . The perfect wurtzite epitaxial structure (HCP structure) of the ZnO (0002) nanowires synthesized on ZnO (002) buffer layer/Si (100) substrate results in excellent optical characteristics such as strong UV emission at 380 nm with potential use in nano-optical and nano-electronic devices.

These ZnO nanowires show excellent field emission properties with turn-on field of 0.83 V/ μm and corresponding current density of 25 $\mu\text{A}/\text{cm}^2$. The emitted current density of the ZnO nanowires is 1.52 mA/ cm^2 at a bias field of 8.5 V/ μm . The large field emission area factor, β arising from the morphology of the nanowire field emitter, is partly responsible for the good emission characteristics.

The Sn doped ZnO (SZO) nanowires were fabricated by a vapor-liquid-solid (VLS) growth process. The reaction temperature for the formation of the nanowires can be reduced to ~ 100 °C due to Sn doping. The growth direction and morphology of SZO nanowires depend on the amount of Sn, which is attributed to different size between Zn and Sn atoms. The ultra-violet (UV) emission of SZO nanowires varies from 380 to 396 nm since Sn acts as a doubly ionized donor and introduces deep states in the band gap. In addition, the SZO nanowires exhibit significantly improved field emission characteristics with a turn-on electric field of 0.05 V/ μm under a current density of 0.5 mA/ cm^2 in comparison with undoped ZnO nanowires. The work function of the SZO nanowire decreases for the higher carrier concentration and the field enhancement factor increases for the smaller diameters.

The metal oxide NWs, especially ZnO NWs have potentials for much field application such as field emission display arrays or optical emission. Furthermore, the studies of the ZnO NWs are still narrow focus on the electric and optical applications. In the future, there are many kinds of subjects could be study which will increase the speed of commercialize.

致謝

一切 是生命裡的一次轉彎。

桌上的雜亂如往常散落，工作與實驗的結束還是詫異的很難想像，滿滿的在心裡的是許許多多深深的祝福與感謝。曾老師俊元教授的指導與提攜，是最可貴的記憶，林老師鵬教授的細心與關懷是最溫暖的風，口試委員龔教授正、吳教授泰伯、王教授錫福、何教授孟書、陳教授三元多次的論辯與指正，更使得這一份工作愈趨完美。

一千八百二十五個日出與日落，謝謝的是竹湖裏似朝陽的你們，昆平、加星、佳穎、俊安、仁豪、適存、良湘、奎府等等許許多多的賣力演出，因為有你們更是生命裡不能缺少的瘋狂，記得世璋、小懿還有耀仁的絮絮叨叨，因為這樣，才能讓我們的心拉得更緊，手繫得更牢，記得那些一起揮舞的日子，記得那曾經豪氣的歲月，因為我們，也因為唯有我們，是如此的與眾不同獨一無二。

在許多的掌聲背後，默默付出的你們，更是無法遺忘的英雄，謝謝月美阿姨、聯珠阿姨、聖德叔叔、怡蕙姐、湘萍姐、宜珍姊、美莉姐、錫昌哥，感謝你們在堅持完美以及絕對苛求的風範，每每在想要放棄的時候，總是毅不容辭的一肩擎天，奮力的承擔屬於自己的一點點夢想，在奈米世紀的天空裡，因為有你們，所以我們都不是完全孤單的。

謝謝您，是予父親母親最最深也最衷心的感謝，這樣的三個字看來是如此的平凡卻又是這樣的不凡，但願將所有的掌聲與榮耀都予您們所有，因為您們才是最有資格接受與驕傲的。

思毅 於 April 2005
Spulding Hotel, San Francisco

Contents

Chinese Abstract	i
English Abstract	iv
Acknowledgement	vi
Contents	vii
List of Illustrations	xii
List of Tables	xviii



Chapter 1 Introduction

1.0	Preface	1
1.1	Motivation	2
1.2	Material Properties	3
1.2.1	Optical Properties	4
1.2.2	Field Emission Properties	6
1.3	Nano Structure Fabricated of Material	9
1.3.1	Vapor-Liquid-Solid (VLS) Growth Mechanism	10
1.3.2	Solution-Liquid-Solid (SLS) Growth Mechanism	11
1.3.3	Laser-Assisted Catalytic Growth (LCG)	14
1.3.4	Template-Based Synthetic Approaches	16
1.4	Characteristics of Zinc Oxide	17
1.5	Research Objectives of Dissertation	18

Chapter 2 Experiment

2.0	Preface	20
2.1	Introduction	20
2.2	Synthesized of ZnO Nanowires	21
2.2.1	Traditional Process for Synthesized ZnO NWs	21
2.2.2	Two-Step Vapor-Liquid-Solid (VLS) Process for Synthesized ZnO NWs	21
2.2.3	Deposited of the ZnO Buffer Layer	22
2.2.4	The Sn Doped ZnO NWs	23
2.2.5	The Sn Doped In_2O_3 NWs	23
2.3	Characteristics of ZnO Nanowires	24
2.3.1	Materials Analysis for ZnO NWs	25
2.3.1.1	Physical Analysis for ZnO NWs	25
2.3.1.2	Chemical Analysis for ZnO NWs	27
2.3.2	Photoluminescence Characteristics for ZnO NWs	29
2.3.3	Field Emission Properties for ZnO NWs	30
2.3.4	Turn-on Electrical Field and Fowler-Nordheim Tunneling (F-N Tunneling)	31
2.4	Summary	38

Chapter 3***Synthesized ZnO Nanowires by VLS Process Using Cu Catalyst***

3.0	Preface	39
3.1	Introduction	39
3.2	Processes of the Synthesized ZnO NWs	40
3.3	The Characteristics of Cu Catalytic ZnO NWs	41

3.3.1	The Different Geometry of The ZnO NWs	41
3.3.2	The Properties of PL of The ZnO NWs	45
3.4	Summary	48

Chapter 4 *Synthesized ZnO Nanowires by VLS Process Under Different Ambient*

4.0	Preface	50
4.1	Introduction	50
4.2	The Different Ambient Ar and N ₂	51
4.3	Characteristics of ZnO NWs Under Different Ambient	52
4.4	Summary	64

Chapter 5 *ZnO Buffer Layer for the Synthesized of ZnO Nanowires*

5.0	Preface	65
5.1	Introduction	65
5.2	Experimental	66
5.3	Results and Discussion	67
5.4	Summary	73

Chapter 6 *Field Emission and Photo Fluorescent Characteristics of Zinc Oxide Nanowires Synthesized by a Metal Catalyzed Vapor-Liquid-Solid Process*

6.0	Preface	74
6.1	Introduction	75
6.2	Experimental	75
6.3	Results and Discussion	77
6.4	Summary	87

Chapter 7	<i>Effect of Sn Dopant on the Properties of ZnO Nanowires</i>	
7.0	Preface	89
7.1	Introduction	89
7.2	Experimental	91
7.3	Results and Discussion	92
7.4	Summary	109
Chapter 8	<i>Low Temperature Synthesized Sn Doped Indium Oxide Nanowires</i>	
8.0	Preface	110
8.1	Introduction	111
8.2	Experimental	112
8.3	Results and Discussion	113
8.4	Summary	127
Chapter 9	<i>Gate Controlled ZnO Nanowires Triode Field Emission Devices (ZnO NWs TFED)</i>	
9.0	Preface	129
9.1	Introduction	130
9.2	Fabricated Process and Structure	131
9.3	Results and Discussion	133
9.3.1	The Characteristics of Material Analysis of Gate Controlled ZnO NWs TFED	133
9.3.2	The Field Emission Properties of Gate Controlled ZnO NWs TFED	136
9.4	Summary	141

Chapter 10 Conclusions

10.0	Conclusion	143
10.1	Future Works and Suggestions	146

<i>References</i>	148
--------------------------	-----



List of Illustrations

Chapter 1 Introduction

Figure 1.1	The nanostructure and their corresponding density of states.	7
Figure 1.2	Energy band diagram for (a) n type nanowire and (b) p type nanowire in electric fields showing electron and hole tunneling, respectively.	9
Figure 1.3	The VLS growth mechanism: the droplet is a metal such as Au, Ag, Pd, Pt, Ni, or Cu, and E ₁ and E ₂ are elements of the crystal phase dissolved in the metallic flux droplet.	11
Figure 1.4	Crystal growth pathway: (a) growth by reversible deposition from solution, liquid or vapor [condition (1)] (b) growth by irreversible deposition with high solid-phase atomic mobility [condition (2)] (c)SLS mechanism: the flux droplet is In, M and E are elements dissolved in the flux droplet. The crystalline fiber and attached flux droplet are suspended in the solution.	13
Figure 1.5	The Si nanowires growth by SLS mechanism.	14
Figure 1.6	Schematic of the LCG growth apparatus.	15
Figure 1.7	The LCG growth mechanism.	15

Chapter 2 Experiment

Figure 2.1	The field emission measurement system with illustration for details.	31
Figure 2.2	Energy band diagram showing the effect of strong electroststic field on the height of the surface potential barrier.	33
Figure 2.3	Energy band diagram showing the electron moving toward a potential barrier with (a) no external electric field, and (b) an external electric field.	35
Figure 2.4	Fowler-Nordheim plot of the current-voltage characteristic of a typical nanowires at room temperature.	38

Chapter 3	Synthesized ZnO NWs by VLS Process Using Cu Catalyst	
Figure 3.1	FE-SEM images of ZnO NWs: (a) tilt 45° view. (b) top view. (c) Growth on 70 Å thickness copper film growth. (d) Growth on 150 Å thickness copper film growth.	42
Figure 3.2	XRD patterns of ZnO NWs of diameters (a) 170-200 nm and (b) 80-150 nm.	43
Figure 3.3	AFM images of copper films after thermal annealing process: (a) 70 Å thick copper film. (b) 150 Å copper film.	44
Figure 3.4	XPS spectra of ZnO NWs (a) scanned from 0 to 1400 eV. (b) binding energy of Zn _{2p1} and Zn _{2p3} . (c) binding energy of O _{1s} .	46
Figure 3.5	HR-TEM image of a single crystalline ZnO nanowire showing the lattice frings. The SAED patterns (inset) along (10 [−] 10) direction.	47
Figure 3.6	Emission spectrum of ZnO NWs using 325 nm incident Xe lamp at room temperature.	48
Chapter 4	Synthesized ZnO Nanowires by VLS Process Under Different Ambient	
Figure 4.1	SEM images of the ZnO nanowires synthesized at 900°C for 3 min. The nanowires shown in (a) and (b) were synthesized in N ₂ , while (c) and (d) in Ar.	53
Figure 4.2	The nanowires length vs. growth time for ZnO nanowires grown in different carrier gases Ar and N ₂ .	54
Figure 4.3	Schematic sketch of the chemical vapor deposition growth process for ZnO nanowires.	57
Figure 4.4	TEM image of the quenched ZnO nanowire. The corresponding electron diffraction pattern is shown in inset.	59
Figure 4.5	TEM bright view images and HRTEM images of the nanowires synthesized in Ar ((a) and (b)) and in N ₂ ((c) and (d)).	61
Figure 4.6	EDX spectra of (a) stem (b) tip of the nanowires grown with N ₂ .	62
Figure 4.7	XPS spectra of the ZnO nanowires synthesized in N ₂ .	62
Figure 4.8	AES spectra of the ZnO nanowires synthesized in N ₂ .	63
Figure 4.9	XRD patterns of ZnO nanowires synthesized in (a) Ar and (b)	63

N₂.

Figure 4.10 Photoluminescence spectra of ZnO nanowires grown in (a) N₂ 64 and (b) Ar at room temperature.

Chapter 5 *ZnO Buffer Layer for the Synthesized of ZnO Nanowires*

Figure 5.1 XRD patterns recorded for the (a) ZnO nanowires on Si (100) substrate, (b) ZnO thin film on Si (100) substrate, and (c) ZnO nanowires on ZnO thin film/Si (100) substrate. 68

Figure 5.2 SEM micrographs of (a) ZnO nanowires grown randomly on Si substrate, (b) ZnO nanowires vertically grown on ZnO film/Si substrate, (c) vertical ZnO nanowires grown for 3 min., and (d) vertical ZnO nanowires. 69

Figure 5.3 XPS spectra of ZnO nanowires of (a) peaks of Zn, and (b) a peak of O. grown for 6 min. 69

Figure 5.4 AES profiles of ZnO nanowires. 70

Figure 5.5 EDS spectra of the ZnO nanowires. The inset shows the line scanning Zn/O ratio of ~49/51 along the longitudinal direction. 71

Figure 5.6 HR-TEM micrographs of ZnO nanowires of (a) the TEM image of a single crystalline ZnO nanowire showing the lattice fringes, (b) the TEM picture of ZnO nanowires showing the geometrical parameters, length and diameter, and (c) the SAED pattern along (10¹0) direction. 72

Figure 5.7 PL emission spectra of ZnO nanowires and film on various substrates using incident Xe lamp excitation at room temperature. 73

Chapter 6 *Field Emission and Photo Fluorescent Characteristics of Zinc Oxide Nanowires Synthesized by a Metal Catalyzed Vapor-Liquid-Solid Process*

Figure 6.1 AFM images of the (a) Au and (b) Cu thin film surface after heating process. 79

Figure 6.2 Schematic illustration of VLS nanowire growth mechanism (a) metal film deposition, (b) metal nanoparticles formation, (c) absorption and nucleation, (d) epitaxial growth. 79

Figure 6.3 FESEM photographs for (a) Au and (b) Cu catalyzed ZnO 80

nanowires synthesized on p-type Si (100) substrate with adopting CGFP method.		
Figure 6.4	XRD patterns of ZnO nanowires synthesized with (a) Au as the catalyst, (b) Au as the catalyst by CGFP method, and (c) Cu as the catalyst by CGFP method.	82
Figure 6.5	HRTEM image of Cu catalyzed ZnO nanowires. The selected area electron diffraction (SAED) pattern is shown in inset (a), while bright view image for side wall of the ZnO nanowires, is indicated in inset (b).	82
Figure 6.6	Typical AES spectrum of Cu catalyzed ZnO nanowires.	85
Figure 6.7	(a) PL spectra of the ZnO nanowires grown on the p-type Si substrate.(b) Tauc's plot of the ZnO nanowires grown on the P-type Si Substrate.	85
Figure 6.8	Field emission characteristics of the ZnO nanowires grown on p-type Si substrates. The inset reveals the F-N plots of the ZnO nanowires.	86
Chapter 7	<i>Effect of Sn Dopant on the Properties of ZnO Nanowires</i>	
Figure 7.1	XRD patterns of the (a) ZnO, (b) 0.1, and (c) 0.3 SZO nanowires. The inset is (0002) peak shifted by Sn dopant.	93
Figure 7.2	SEM images of the (a) ZnO, (b) 0.1, and (c) 0.3 SZO nanowires.	95
Figure 7.3	VLS growth process mechanism for, (a) undoped, (b) 0.1 and (c) 0.3 SZO nanowires.	97
Figure 7.4	(a) HR-TEM images of the 0.1 SZO nanowires. The (0002) lattice fringe is tilted by about 70° with growth direction. The inset is SAED pattern. (b) HR-TEM images of the 0.3 SZO nanowires. The (0002) lattice fringe is tilted by about 88° with the growth direction. The inset is SAED pattern. (c) The slip structure with the different molar fractions of Sn in SZO nanowires.	98
Figure 7.5	(a) EDS spectrum of the SZO nanowires and (b) enlarged EDS spectra of the SZO nanowires.	101
Figure 7.6	XPS spectra of the 0.3 Sn doped SZO nanowires, (a) Zn spectrum, (b) O spectrum, and (c) Sn spectrum.	102
Figure 7.7	AES differential spectra of the 0.3 Sn doped SZO nanowires,	103

(a) full scale scanning results. (b) Zn spectrum, (c) O spectrum, and (d) Sn spectrum.		
Figure 7.8		
(a) PL emission spectra of the updoped and SZO nanowires. (b) PL emission curve fitted analysis for 0.3 SZO nanowires. (c) proposed energy band structure of the undoped and the SZO nanowires.	105	
Figure 7.9		
(a) Field emission characteristics of the ZnO, (b) F-N plots of undoped ZnO, (c) F-N plots of 0.1 Sn doped, and (d) F-N plots of 0.3 Sn doped ZnO nanowires.	107	
Figure 7.10		
Emission current density vs. electric field of the undoped, 0.1, and 0.3 SZO nanowires.	108	
Chapter 8	Low Temperature Synthesized Sn Doped Indium Oxide Nanowires	
Figure 8.1	(a) XRD patterns of the SIO NWs at different synthesis temperatures from 770 to 900 °C and (c) the lattice parameter and atomic weight percentage of Sn doped at different synthesis temperatures.	114
Figure 8.2	FE-SEM images of the SIO NWs : (a) large area of the selective synthesized process of SIO NWs, (b) the zoom in photo of the edge of the 100 µm diameter metal mask for selective growth, (c) 45° tilted view for 10 µm length and ~80 nm diameter of the SIO NWs at central region and (d) is the outside region near the circle of SIO NWs growth.	117
Figure 8.3	TEM photograph of a single crystalline SIO NW : (a) Indexed SAED diffraction indexing pattern, (b) bright view of the SIO NW, (c) HR-TEM image showing the lattice frings, (d) simulated SAED pattern that is consistent with (a), (e) IFFT image for (c).	118
Figure 8.4	(a) EDS spectra indicating the elements In, O , and Sn distributions of the SIO NWs, (b) EDS spectrum of Sn peaks of the SIO NWs grown at 770 °C.	120
Figure 8.5	XPS spectra of the SIO NWs: (a) fully scanned from 0 to 1200 eV, (b) high resolution selective spectrum of O, (c) high resolution selective spectrum of In, and (d) high resolution selective spectrum of Sn, respectively.	122
Figure 8.6	Emission spectra of the SIO NWs using 275 nm incident Xe lamp at room temperature (298 K).	123

Figure 8.7 Field emission characteristic of the SIO NWs and the inset is the F-N plot that is calculated from field emission enhancement coefficient. 125

Figure 8.8 Emission current density versus lower electric field of the different temperature 770 and 900 °C grown SIO NWs. 125

Chapter 9 **Gate Controlled ZnO Nanowires Triode Field Emission Devices (ZnO NWs TFED)**

Figure 9.1 The fabrication process for the triode structure for gate controlled ZnO NWs field emission devices. 132

Figure 9.2 Schematic diagram of a high vacuum chamber system for field emission measurement. 132

Figure 9.3 SEM images of ZnO NWs synthesized on the emitter region of the triode. (a) a entirety image for four triode devices of the ZnO NWs and (b) vertically growth ZnO NWs on the emitter region. 134

Figure 9.4 The XRD pattern and HR-TEM images of the ZnO NWs. (a) the XRD pattern presents the (002) prefer orientation ZnO NWs, (b) HR-TEM image indicates the lattice fringes and SAED image on the inset, and (c) the EDS patterns for chemical composition of the ZnO NWs. 135

Figure 9.5 The field emission properties for (a) different gate voltage, V_g v.s turn-on electric field and (b) F-N plot for different V_g field emission characteristic. 137

Figure 9.6 (a) The drain current, I_d function of different gate voltage, V_g characteristic curves, (b) I_d v.s. V_g . for gate controlled ZnO NWs field emission device, (c) the F-N plot for different V_g v.s emission current, and (d) transconducance, g_m v.s. different turn-on electric field. 140

List of Tables

Table 8.1 The field emission characteristics of carbon nanotubes (CNTs) 127 and oxide NWs with and without Sn doped.

Table 9.1 The relationships of gate voltage, (V_g), turn-on electric field, 141 (E_{to}) and the field emission enhancement factor, β of the gated controlled ZnO NWs field emission devices.

